www.ietdl.org

Published in IET Wireless Sensor Systems
Received on 22nd December 2010
Revised on 10th February 2012
doi: 10.1049/iet-wss.2011.0178

ISSN 2043-6386

Distributed passive radar sensor networks with near-space vehicle-borne receivers

*W.-Q. Wang**

School of Communication and Information Engineering, University of Electronic Science and Technology of China (UESTC), Chengdu, People's Republic of China, 611731
**State Laboratory of Remote Sensing Science, Institute of Remote Sensing Applications, Chinese Academy of Sciences, Beijing, People's Republic of China, 100101*
E-mail: wqwang@uestc.edu.cn

Abstract: In this study, we propose a distributed passive radar sensor network with near-space vehicle-borne receivers for regional remote sensing surveillance. Note that near-space is referred to the altitude range between 20 and 100 km is too high for airplanes, but too low for satellites. Near-space vehicles can offer a wide coverage like satellite and a fast maneuverability like airplane. The distributed passive radar sensor networks system operation mode, imaging coverage and imaging resolution are analysed. As there is a big speed difference between the transmit and receive platforms, we propose a multi-beamforming and scan-on-receive combined approach to extend the limited imaging coverage. Since the conventional motion compensation technique may be not reachable for the system due to its limited load capability, an overlapped subaperture-based motion compensation algorithm is proposed. The effectiveness of the approaches is validated by numerical simulation results.

1 Introduction

In recent years, radar sensor networks have received enormous research interests [1–7]. Radar sensor networks can enable a technology for potential applications such as surveillance and environment monitoring, which are not accessible for conventional communication networks [8]. In the radar sensor network, each radar sensor can be an independent system which transmits a known waveform and receives the returns. Radar sensor networks can be utilised to obtain an improved performance [9]. They can be arranged to survey a large area and observe targets from a number of different angles. Moreover, radar sensor networks offer to alleviate the blind speed problem that occurs when the Doppler shift is equal to the same or a multiple of the pulse repetition frequency (PRF) [10]. One radar sensor network that works in an *ad hoc* fashion, but is grouped together by an intelligent clusterhead was proposed in [11].

Different from the literature, in this study we propose a distributed passive radar sensor network with near-space vehicle-borne receivers for regional remote sensing surveillance. Although spaceborne and airborne radars have become a valuable remote sensing tool, they are not a good tool that can be used for persistent monitoring because of its low revisiting frequency. Differently, near-space vehicle can supply the gap between satellite and airplane [12]. Therefore, the proposed distributed passive radar sensor network can be used for regionally remote monitoring.

Near-space is referred to the altitude range between 20 and 100 km is too high for airplanes but too low for satellites [13, 14]. However, near-space offers many capabilities that are not accessible for low earth orbit (LEO) satellites and airplanes [15]. Generally speaking, satellites usually operate in the orbits higher than 200 km, and air-breathing airplanes routinely operate lower than 18 km. Consequently there are little sensors in the altitude between airplanes and satellites [16]. Although compared with satellites and airplanes, the vehicles operating in near-space offers three obvious advantages: first, near-space is above troposphere and atmosphere region where most weather occurs, so both stationary and ultrasound speed can be obtained for near-space vehicles. Secondly, not constrained by orbital mechanics like satellites or high fuel consumption like airplanes, they can stay at a specific site almost indefinitely to provide a persistent region coverage. Thirdly, they are low cost. Their inherent simplicity, recoverability and without space-hardening requirements all contribute into this advantage. These advantages provide promising potentials for some specific remote sensing applications [17, 18]. Thus, near-space has received much attention in recent years and why several types of near-space vehicles are being studied, developed or employed [19–23].

The proposed radar sensor network can be seen as a kind of distributed radar system. The interest in distributed radars has rapidly increased in recent years [24, 25]. This is based on the specific advantages of bistatic configuration when comparison with monostatic configuration. However, most of the distributed radar systems investigated in the literature are azimuth-invariant configurations [26], in which the transmitter and the receiver are moving along parallel trajectories with the same velocity. The distributed passive radar sensor network considered in this paper has an azimuth-variant configuration where the transmitter and the receiver have different trajectories or velocities. Consequently the Doppler signal will be azimuth-variant. It is thus necessary to analyse the corresponding system performance. On the contrary, conventional motion compensation algorithm cannot be employed for the system because the near-space vehicles have only limited load capability and motion compensation algorithm is required.

The remaining sections are organised as follows. In Section 2, the system parameters and imaging performance are analysed. Next, Section 3 presents the overlapped subaperture-based motion compensation technique. Section 4 designs the conceptual system and provides the simulation results. Finally, Section 5 concludes the whole study.

2 Distributed passive radar sensor network via near-space vehicle-borne receivers

The distributed passive radar sensor network involves placing a receiver inside a near-space vehicle and utilising opportunistic transmitters such as spaceborne and airborne radar sensor. Fig. 1 shows an example geometry of the passive radar sensor network. Although the near-space vehicle-borne receiver may be stationary, an aperture synthesis can still be obtained by the transmitter motion only. The near-space vehicle-borne receiver consists of two channels. One channel is fixed to collect the direct-path signals coming from the transmitter antenna sidelobes, which is used as the reference function for matched filtering and synchronisation compensation [27]. The other channel is configured to gather the reflected signals with which navigation and surveillance are attempted.

2.1 Operational mode and system parameters

As distributed radar sensor networks can be represented by bistatic radars, we consider only the bistatic radars in the following discussions. Near-space vehicle-borne bistatic radars can operate in strip, spotlight and scan modes. Without loss of generality, only strip mode using spaceborne transmitter is considered in the following sections. Suppose the transmitter and the receiver are flying with a parallel trajectory but at unequal velocities. Consider Fig. 1 (Tx and Rx denote the transmitter and receiver, respectively), as only the volume common to both transmit and receive beams can be imaged, the overlap time T_{overlap} is limited by

$$T_{\text{overlap}} = \frac{|W_{\text{az,t}} - W_{\text{az,r}}|}{|v_{\text{t}} - v_{\text{r}}|} \tag{1}$$

where $W_{\text{az,t}}$ and $W_{\text{az,r}}$ are the ground coverage in azimuth for the transmitter and the receiver, v_{t} and v_{r} are the velocity for the transmitter and the receiver (Fig. 2).

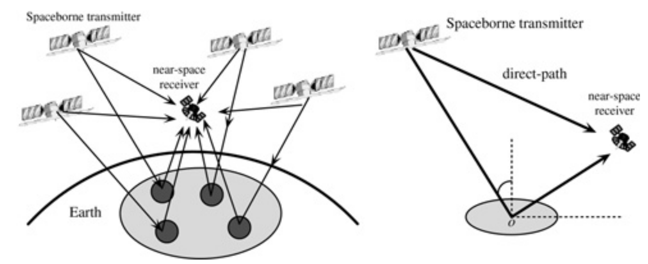

Fig. 1 *Geometry of the passive radar sensor network with near-space vehicle-borne receivers and spaceborne transmitter*

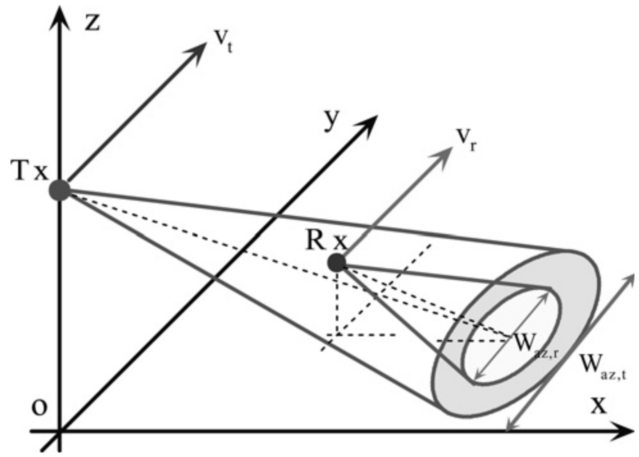

Fig. 2 *Illustration of the overlapped swath covered by the transmitter and receiver*

There are two parameters on the transmitter side, which have an influence on the imaging time during which the area of interest can be illuminated. The first parameter is the transmitter velocity, which is very high relative to the receiver. The second transmitter parameter is the very small antenna steering range in azimuth. To increase the scene extension in azimuth, the receiver must perform antenna steering. One pulse chasing technique is proposed in [28], but it cannot be easily implemented for non-cooperative bistatic radar configurations. An approach involving transmitter sliding spotlight in transmitter and receiver footprint chasing is proposed for spaceborne/airborne bistatic radar systems in [29]. Owing to the fact that antenna steering is employed in both the transmitter and the receiver, it is difficult to develop the subsequent image formation algorithms. Moreover, the satellite antenna direction is often uncontrollable for us. To overcome these disadvantages, we can use a wide antenna beamwidth on receive due to its advantage of high signal-to-noise ratio (SNR).

The bistatic radar equation is given by [30]

$$P_{\text{r}} = \frac{P_{\text{t}}\lambda^2 G_{\text{t}} G_{\text{r}} \sigma_{\text{b}}^{\text{o}} A_{\text{res}}}{(4\pi)^3 R_{\text{t}}^2 R_{\text{r}}^2} \tag{2}$$

where P_{t} and P_{r} are the average transmit and receive power, λ is the wavelength, G_{t} and G_{r} are the gain of the transmit and the receiver antenna, R_{t} and R_{r} are the distance from the transmitter and receiver to the imaged scene, $\sigma_{\text{b}}^{\text{o}}$ is the bistatic scattering coefficient and A_{res} is the size of the resolution cell. The SNR in receiver can then be represented by

$$\text{SNR}_b = \frac{P_{\text{t}}\lambda^2 G_{\text{t}} G_{\text{r}} \sigma_{\text{b}}^{\text{o}} A_{\text{res}} \zeta_{\text{int}} \eta}{(4\pi)^3 R_{\text{t}}^2 R_{\text{r}}^2 K_0 T_0 F_{\text{n}}} \tag{3}$$

where ζ_{int} is the coherent integration time, η is the duty cycle, K_{B} is the Boltzmann constant, T_0 is the system noise temperature and F_{n} is the noise figure.

Simplify, we suppose the transmitter and the receiver are flying in a parallel trajectory (but their flying velocity are not equal), then the size of the resolution cell is expressed as

$$A_{\text{res}} = \frac{\lambda}{v_{\text{t}}/R_{\text{t}} + v_{\text{r}}/R_{\text{r}}} \times \frac{1}{\zeta_{\text{int}}} \times \frac{c_0}{2B_{\text{r}}\cos(\beta/2)\sin(\gamma_{\text{b}})} \tag{4}$$

IET Wirel. Sens. Syst., 2012, Vol. 2, Iss. 3, pp. 183–190
doi: 10.1049/iet-wss.2011.0178

where v_t (v_r) is the transmitter (receiver) velocity, R_t (R_r) is the transmitter-to-target (target-to-receiver) distance, c_0 is the speed of light, B_r is the transmitted signal bandwidth, β is the bistatic angle and γ_b is the incidence angle of the bistatic angle bisector [31]. Equation (3) can then be changed into

$$\mathrm{SNR_b} = \frac{P_t\lambda^2 G_t G_r \sigma_b^o \eta}{(4\pi)^3 R_t^2 R_r^2 K_B T_0 F_n} \times \frac{\lambda}{v_t/R_t + v_r/R_r} \times \frac{c_0}{2B_r\cos(\beta/2)\sin(\gamma_b)} \quad (5)$$

Similarly, for the corresponding monostatic spaceborne radar, there is

$$\mathrm{SNR_m} = \frac{P_t\lambda^2 G_t^2 \sigma_m^o \eta}{(4\pi)^3 R_t^4 K_B T_s F_n} \times \frac{\lambda}{2v_t/R_t} \times \frac{c_0}{2B_r\sin(\gamma_m)} \quad (6)$$

where σ_m^o and γ_m are the monostatic scattering coefficient and radar incidence angle, respectively. Note that, here equal system noise temperature and noise figure are assumed. We then have

$$K_\mu = \frac{\mathrm{SNR_b}}{\mathrm{SNR_m}} = \frac{G_r}{G_t}\left(\frac{R_t}{R_r}\right)^2 \frac{2v_t/R_t}{v_t/R_t + v_r/R_r} \times \frac{\sigma_b^o}{\sigma_m^o} \times \frac{\sin(\gamma_m)}{\cos(\beta/2)\sin(\gamma_b)} \quad (7)$$

As an example, supposing the following parameters: $R_t = 800$ km, $v_t = 7000$ m/s, $R_r = 30$ km, $v_r = 5$ m/s, $\gamma_b = 45^\circ$, $\gamma_m = 60^\circ$, $\beta = 30^\circ$ and $\sigma_b^o = \sigma_m^o$, the K_μ is found to be $1973.70G_r/G_t$. This points out that the receiver antenna beamwidth can be significantly extended to provide the same SNR in comparison to the monostatic case [32]; hence, an extended bistatic radar imaging coverage can be obtained by extending the beamwidth of the near-space vehicle-borne receiver antenna.

To ensure the transmitter and the receiver have common beam coverage, the synthetic aperture time is limited by

$$T_s = \min\left\{\frac{\lambda R_{t0}}{L_t v_t}, \frac{\lambda R_{r0}}{L_r v_r}\right\} \quad (8)$$

where R_{t0} and R_{r0} are the nearest slant range for the transmitter and the receiver, L_t and L_r denote the transmitting and the receiving antenna length. In the case that spaceborne transmitter is employed, there should be

$$L_r \le \rho_a, \quad L_t \le R_{t0} D_r / R_{r0} \quad (9)$$

Considering the geometry shown in Fig. 3, the transmitting and receiving antenna width D_t and D_r are determined, respectively, by

$$\begin{cases} D_t = \lambda/\theta_t \\ \theta_t = W_r\cos(\phi_t)/R_{t0} \\ R_{t0} = h_t/\cos(\phi_t) \end{cases} \quad (10)$$

$$\begin{cases} D_r = \lambda/\theta_r \\ \theta_r = W_r\cos(\phi_r)/R_{r0} \\ R_{r0} = h_r/\cos(\phi_r) \end{cases} \quad (11)$$

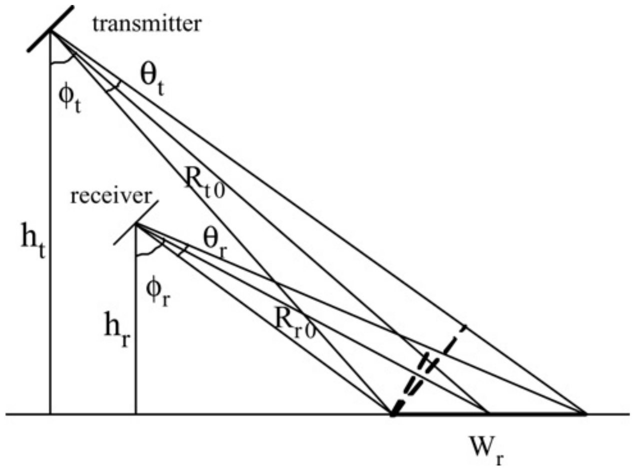

Fig. 3 *Geometry of the relations between transmit and receive beams*

The corresponding imaging swath W_r is determined by

$$W_r = \frac{c_0}{\mathrm{PRF}} \times \frac{1}{(\sin(\phi_t)/\sin(\theta_t/2)) + (\sin(\phi_r)/\sin(\theta_r/2))} \quad (12)$$

where c_0 and PRF denote the speed of light and PRF, respectively.

2.2 Imaging spatial resolution

From Fig. 3 we know that the instantaneous range history of the transmitter and the receiver to an arbitrary point target $(x, y, 0)$ is

$$R = \sqrt{(x-x_t)^2 + (y-y_t)^2 + h_t^2} + \sqrt{(x-x_r)^2 + (y-y_r)^2 + h_r^2} \quad (13)$$

where (x_t, y_t, h_t) and (x_r, y_r, h_r) are the coordinates of the transmitter and the receiver, respectively. We then have

$$\begin{aligned}\nabla R &= \frac{\partial R}{\partial x}\boldsymbol{i}_x + \frac{\partial R}{\partial y}\boldsymbol{i}_y \\ &= [\sin(\boldsymbol{\alpha}_t)\cos(\boldsymbol{\zeta}_t) + \sin(\boldsymbol{\alpha}_r)\cos(\boldsymbol{\zeta}_r)]\boldsymbol{i}_x \\ &\quad + [\sin(\boldsymbol{\zeta}_t) + \sin(\boldsymbol{\zeta}_r)]\boldsymbol{i}_y \end{aligned} \quad (14)$$

where $\alpha_t = \alpha_t(x)$ and $\alpha_r = \alpha_r(x)$ are the instantaneous looking-down angles, $\zeta_t = \zeta_t(x, y, y_t)$ and $\zeta_r = \zeta_r(x, y; y_r)$ (y_t, y_r is the instantaneous location in y-direction) are the instantaneous squint angles. There is

$$|\nabla R| = \sqrt{[\sin(\boldsymbol{\alpha}_t)\cos(\boldsymbol{\zeta}_t) + \sin(\boldsymbol{\alpha}_r)\cos(\boldsymbol{\zeta}_r)]^2 + [\sin(\boldsymbol{\zeta}_t) + \sin(\boldsymbol{\zeta}_r)]^2} \quad (15)$$

As the range resolution of a monostatic radar is $c_0/2B_r$ with B_r the transmit signal bandwidth, the range resolution of near-space vehicle-borne bistatic radar can then be derived as

$$\rho_{\rm r} = \frac{c_0/B_{\rm r}}{\nabla R} \times \frac{1}{\sin(\xi_{xy})} \tag{16}$$

with

$$\xi_{xy} = \arctan\left(\frac{\sin(\xi_{\rm t}) + \sin(\xi_{\rm r})}{\sin(\alpha_{\rm t})\cos(\xi_{\rm t}) + \sin(\alpha_{\rm r})\cos(\xi_{\rm r})}\right) \tag{17}$$

We then have

$$\rho_{\rm r} = \frac{c_0/B_{\rm r}}{\sin(\alpha_{\rm t})\cos(\xi_{\rm t}) + \sin(\alpha_{\rm r})\cos(\xi_{\rm r})} \tag{18}$$

Unlike the monostatic cases, the range resolution is determined by not only the transmitted signal bandwidth, but also the specific bistatic radar configuration geometry.

To investigate the azimuth resolution, we consider the range history to an arbitrary reference point at an azimuth time τ

$$R_{\rm b}(\tau) = \sqrt{R_{\rm t0}^2 + (v_{\rm t}\tau)^2} + \sqrt{R_{\rm r0}^2 + (v_{\rm r}\tau)^2} \tag{19}$$

As the propagation speed of electromagnetic signal is much faster than the speed of platforms, here the stop-and-go hypothesis [33] is still reasonable. The instantaneous Doppler chirp rate is derived as

$$\begin{aligned} k_{\rm d}(\tau) &= -\frac{1}{\lambda} \times \frac{\partial^2 R_{\rm b}(\tau)}{\partial^2 \tau} \\ &\simeq -\frac{1}{\lambda}\left[\frac{v_{\rm t}^2}{R_{\rm t0}}\cos\left(\frac{v_{\rm t}\tau}{R_{\rm t0}}\right) + \frac{v_{\rm r}^2}{R_{\rm r0}}\cos\left(\frac{v_{\rm r}\tau}{R_{\rm r0}}\right)\right] \end{aligned} \tag{20}$$

The azimuth resolution can then be expressed as

$$\rho_{\rm a} = \frac{\sqrt{v_{\rm t}^2 + v_{\rm r}^2 - 2v_{\rm t}v_{\rm r}\cos(\pi - \gamma)}}{2[(v_{\rm t}/\lambda)\sin(\lambda R_{\rm r0}v_{\rm t}/2L_{\rm r}R_{\rm t0}v_{\rm r}) + (v_{\rm r}/\lambda)\sin(\lambda/2L_{\rm r})]} \tag{21}$$

where γ is defined as the angle between the transmitter and the receiver velocity vectors. If $v_{\rm r} = 0$, this case is just a fixed-receiver bistatic radar [34].

3 Overlapped subaperture-based motion compensation

In the previous discussions, we did not consider the motion errors. For a short coherent processing interval, we ignore the acceleration errors in along-track and consider only the motion errors in cross-track in the following discussions. As shown in Fig. 4, suppose the ideal transmitter and the receiver instantaneous positions at azimuth time $\tau_{\rm m}$ are $(v_{\rm t}\tau_{\rm m}, y_{\rm t0}, h_{\rm t})$ and $(v_{\rm r}\tau_{\rm m}, y_{\rm r0}, h_{\rm r})$, respectively, but their actual positions are $(v_{\rm t}\tau_{\rm m}, y_{\rm t0} + \Delta y_{\rm t}(\tau_{\rm m}), h_{\rm t})$ and $(v_{\rm r}\tau_{\rm m}, y_{\rm r0}\Delta y_{\rm r}(\tau_{\rm m}), h_r)$.

Suppose the transmitter motion error in the cross-track is $\Delta r_{\rm t}(\tau_{\rm m})$, there are $\Delta y_{\rm t}(\tau_{\rm m}) = -\Delta r_{\rm t}(\tau_{\rm m})\cos(\alpha_{\rm t0})$ ($\alpha_{\rm t0}$ is the instantaneous incidence angle from the transmitter to the point target $P_{\rm n}(x_{\rm n}, y_{\rm n}, 0)$), $\Delta z_{\rm t}(\tau_{\rm m}) = -\Delta r_{\rm t}(\tau_{\rm m})\sin(\alpha_{\rm t0})$ and $y_{\rm n} - y_{\rm t0} = r_{\rm tn}\cos(\alpha_{\rm t0})$ with $r_{\rm tn} = \sqrt{h_{\rm t}^2 + (y_{\rm n} - y_{\rm t0})^2}$ and

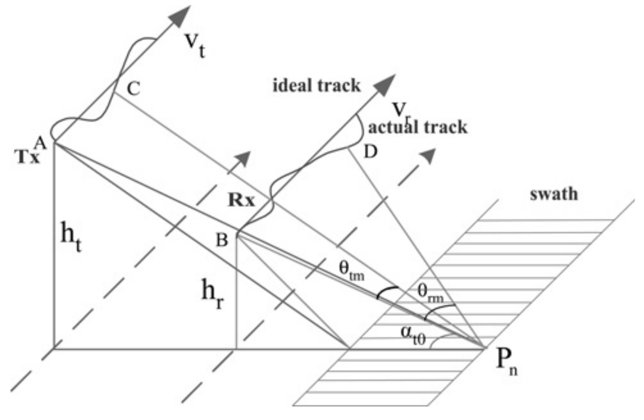

Fig. 4 *Illustration of the relative motion errors between the transmitter and receiver*

$h_{\rm t} = r_{\rm tn}\sin(\alpha_{\rm t0})$. The transmitter range history can then be represented by

$$\begin{aligned} &R_{\rm t}(\tau_{\rm m}) \\ &= \sqrt{(x_{\rm n} - v_{\rm t}\tau_{\rm m})^2 + (y_{\rm n} - y_{\rm t0} - \Delta y_{\rm t}(\tau_{\rm m}))^2 + (h_{\rm t} - \Delta z_{\rm t}(\tau_{\rm m}))^2} \\ &= \sqrt{(x_{\rm n} - v_{\rm t}\tau_{\rm m})^2 + r_{\rm tn}^2 + 2r_{\rm tn}(\Delta r_{\rm t}(\tau_{\rm m}) + \Delta r_{\rm t}^2(\tau_{\rm m}))} \end{aligned} \tag{22}$$

Assume the instantaneous transmitter squint angle is $\theta_{\rm tm}$ and denote $x_{\rm t}(\tau_{\rm m}) = x_{\rm n} - v_{\rm t}\tau_{\rm m}$ and $\tan(\theta_{\rm tm}) = x_{\rm t}(\tau_{\rm m})/r_{\rm tn}$, we can then get

$$\begin{aligned} R_{\rm t}(\tau_{\rm m}) &= \sqrt{r_{\rm tn}^2 + x_{\rm t}^2(\tau_{\rm m})} - \Delta r_{\rm t}(\tau_{\rm m})\cos(\theta_{\rm tm}) \\ &\quad + \sin(\theta_{\rm tm})\sin(2\theta_{\rm tm})\frac{\Delta r_{\rm t}^2(\tau_{\rm m})}{2r_{\rm tn}} + O\left(\frac{\Delta r_{\rm t}(\tau_{\rm m})}{r_{\rm tn}}\right) \\ &\simeq \sqrt{r_{\rm tn}^2 + x_{\rm t}^2(\tau_{\rm m})} - \Delta r_{\rm t}(\tau_{\rm m})\cos(\theta_{\rm tm}) \end{aligned} \tag{23}$$

Similarly, for the receiver range history we have

$$R_{\rm r}(\tau_{\rm m}) \simeq \sqrt{r_{\rm rn}^2 + x_{\rm r}^2(\tau_{\rm m})} - \Delta r_{\rm r}(\tau_{\rm m})\cos(\theta_{\rm rm}) \tag{24}$$

where $r_{\rm rn}$, $x_{\rm r}(\tau_{\rm m})$, $\Delta r_{\rm r}(\tau_{\rm m})$ and $\theta_{\rm rm}$ are are defined in an alike manner as the $r_{\rm tn}$, $x_{\rm t}(\tau_{\rm m})$, $\Delta r_{\rm t}(\tau_{\rm m})$ and $\theta_{\rm tm}$. The bistatic range history can then be represented by

$$\begin{aligned} R_{\rm b}(\tau_{\rm m}) &\simeq \sqrt{r_{\rm tn}^2 + x_{\rm t}^2(\tau_{\rm m})} - \Delta r_{\rm t}(\tau_{\rm m})\cos(\theta_{\rm tm}) \\ &\quad + \sqrt{r_{\rm rn}^2 + x_{\rm r}^2(\tau_{\rm m})} - \Delta r_{\rm r}(\tau_{\rm m})\cos(\theta_{\rm rm}) \end{aligned} \tag{25}$$

As the first and third terms are the ideal range history for subsequent image formation processing, we consider only the second and fourth terms. We have

$$\begin{aligned} &\frac{\partial[\Delta r_{\rm t}(\tau_{\rm m})\cos(\theta_{\rm tm}) + \Delta r_{\rm r}(\tau_{\rm m})\cos(\theta_{\rm rm})]}{\partial \tau_{\rm m}} \\ &= -\frac{\Delta r_{\rm t}(\tau_{\rm m1})}{r_{\rm tn}}\sin(\theta_{\rm tm}) \times v_{\rm t} \times (\tau_{\rm m2} - \tau_{\rm m1}) \\ &\quad - \frac{\Delta r_{\rm r}(\tau_{\rm m1})}{r_{\rm rn}}\sin(\theta_{\rm rm}) \times v_{\rm r} \times (\tau_{\rm m2} - \tau_{\rm m1}) \end{aligned} \tag{26}$$

doi: 10.1049/iet-wss.2011.0178

As there are $\Delta r_t(\tau_{m1})/r_{tn} = 1$ and $\Delta r_r(\tau_{m1})/r_{rn} = 1$, when $\tau_{m2} - \tau_{m1}$ is short, (26) will be equal to zero. Therefore, we present a subaperture-based motion compensation algorithm.

It can easily be derived that the Doppler signal received by each radar sensor can be represented by

$$G_B(f) = \exp\left(j\pi\frac{f^2}{k_a}\right), \quad -\frac{B_a}{2} < f < \frac{B_a}{2} \tag{27}$$

where f is the Doppler frequency, B_a is the Doppler bandwidth and k_a is the Doppler chirp rate. As shown in Fig. 4, we divide the azimuth Doppler data into multiple (N) subapertures, each subaperture has a bandwidth of B_{as}. Consider two adjacent subapertures

$$G_{L_i}(f) = G_B\left(f - \frac{B_{as}}{2}\right) = \exp\left(j\pi\frac{(f - (B_{as}/2))^2}{k_a}\right), \quad f_i - \frac{B_a}{2} < f < f_i + \frac{B_a}{2} \tag{28}$$

$$G_{H_i}(f) = G_B\left(f + \frac{B_{as}}{2}\right) = \exp\left(j\pi\frac{(f + (B_{as}/2))^2}{k_a}\right), \quad f_i - \frac{B_a}{2} < f < f_i + \frac{B_a}{2} \tag{29}$$

We then have

$$G_{m_i}(f) = G_{L_i}(f)G^*_{H_i}(f) = \exp\left(-j2\pi\frac{B_{as}}{k_a}f\right), \quad f_i - \frac{B_a}{2} < f < f_i + \frac{B_a}{2} \tag{30}$$

Applying an inverse Fourier transform, we get

$$g_{m_i}(t) = \text{sinc}\left(t_i - \frac{B_{as}}{k_a}\right) \tag{31}$$

The maxima arrives at $t_i = B_{as}/k_a$. The chirp rate in the ith subaperture can then be estimated as

$$k_a = \frac{B_{as}}{t_i} \tag{32}$$

The detailed processing flow chart of the overlapped subaperture-based motion compensation algorithm is given in Figs. 5 and 6.

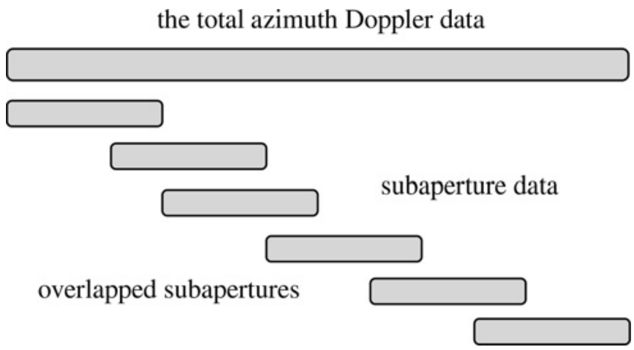

Fig. 5 *Illustration of overlapped azimuth Doppler subapertures*

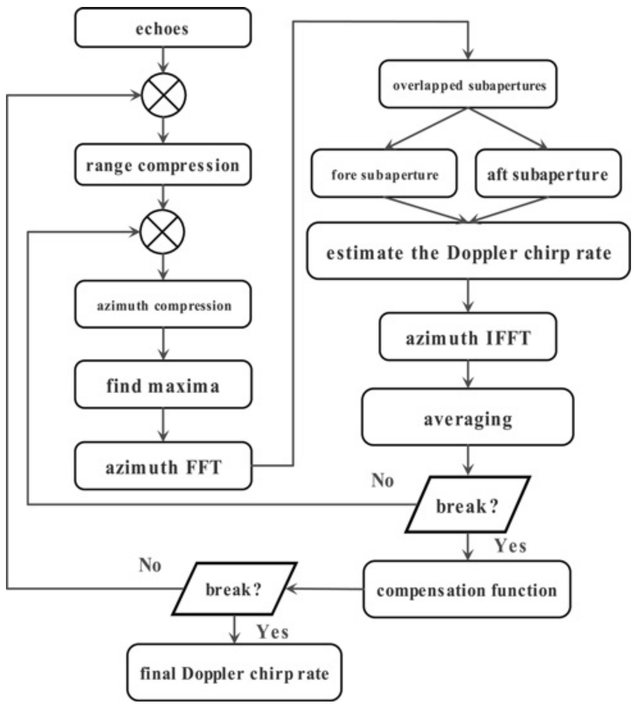

Fig. 6 *Flow chart of the overlapped subaperture-based motion compensation algorithm*

Table 1 Typical system parameters for the radar sensor network with near-space vehicle-borne receivers

Parameters	Tx-A	Rx-A	Tx-B	Rx-B	Tx-C	Rx-C
flying altitude in km	515	20	800	20	645	20
flying velocity in m/s	7600	5	7450	5	7530	5
incidence angle °	45	60	45	60	30	60
carrier frequency in GHz	9.65	9.65	5.33	5.33	1.260	1.26
transmit power in kW	2.26	–	2.30	–	4	–
PRF in Hz	4000	–	2000	–	2000	–
system SNR loss in dB	2	3	2	3	2	3
pulse duration in μs	45	–	25	–	35	–
receiver noise figure in dB	–	5	–	5	–	5
receiver noise temperature in °C	–	300	–	300	–	300
signal bandwidth in MHz	150	–	16	–	85	–
range beamwidth in °C	2.30	10	2.30	10	2.3	15
azimuth beamwidth in °C	0.33	10	0.33	10	0.28	10
imaging scene in km	(4.04, 4.03)	–	(4.04, 4.04)	–	(6.08, 6.07)	–

4 Conceptual systems and simulation results

To obtain quantitative evaluation, we consider the spaceborne radar TerraSAR-X, Envisat and TettaSAR-L as example transmitters, the corresponding typical system parameters are given in Table 1 (Tx-A, Tx-B and Tx-C denote the TerraSAR-X [35], Envisat [36] and TettaSAR-L, respectively. Rx-A/B/C denote three different near-space vehicle-borne receivers). We notice that an imaging scene coverage of dozens of square kilometers (the size is from 4×4 km^2 to 6×6 km^2 in the simulation examples) can be obtained.

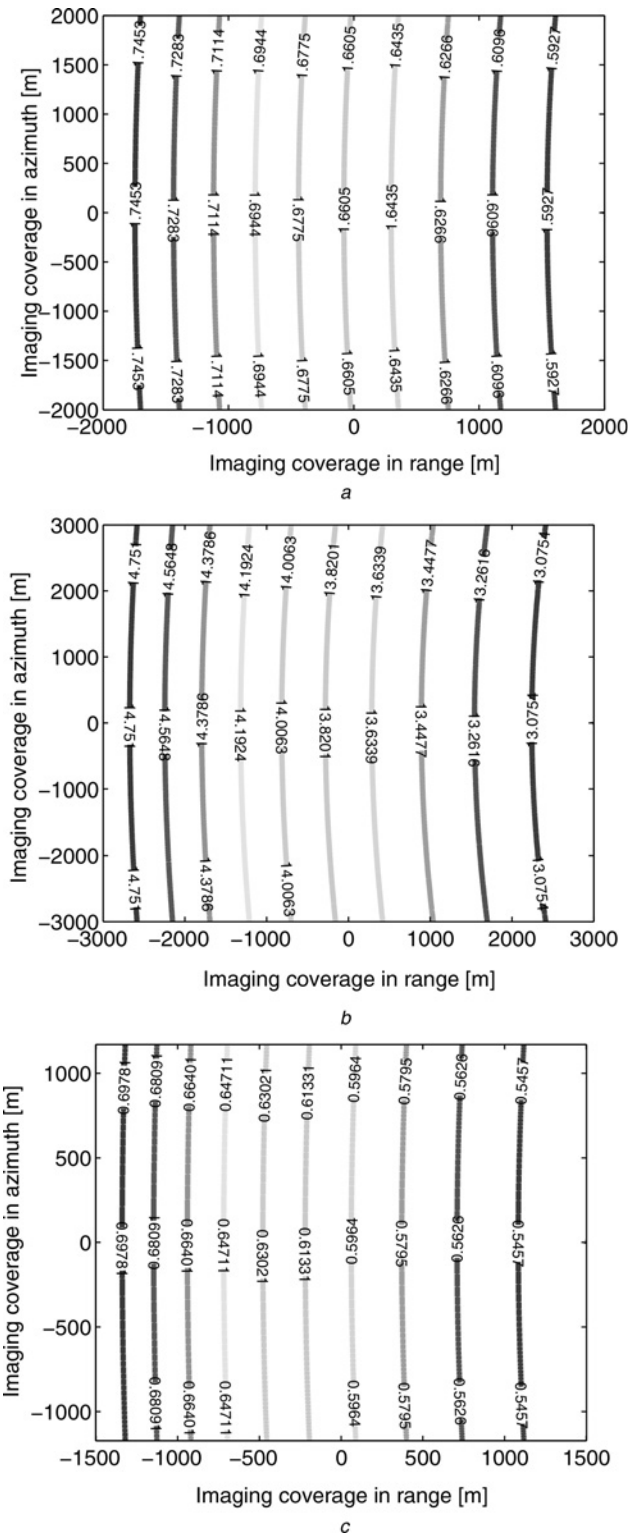

Fig. 7 *Range resolution results of the example transmitter and receiver configurations*

a Case A: Tx-A and Rx-A
b Case B: Tx-B and Rx-B
c Case C: Tx-C and Rx-C

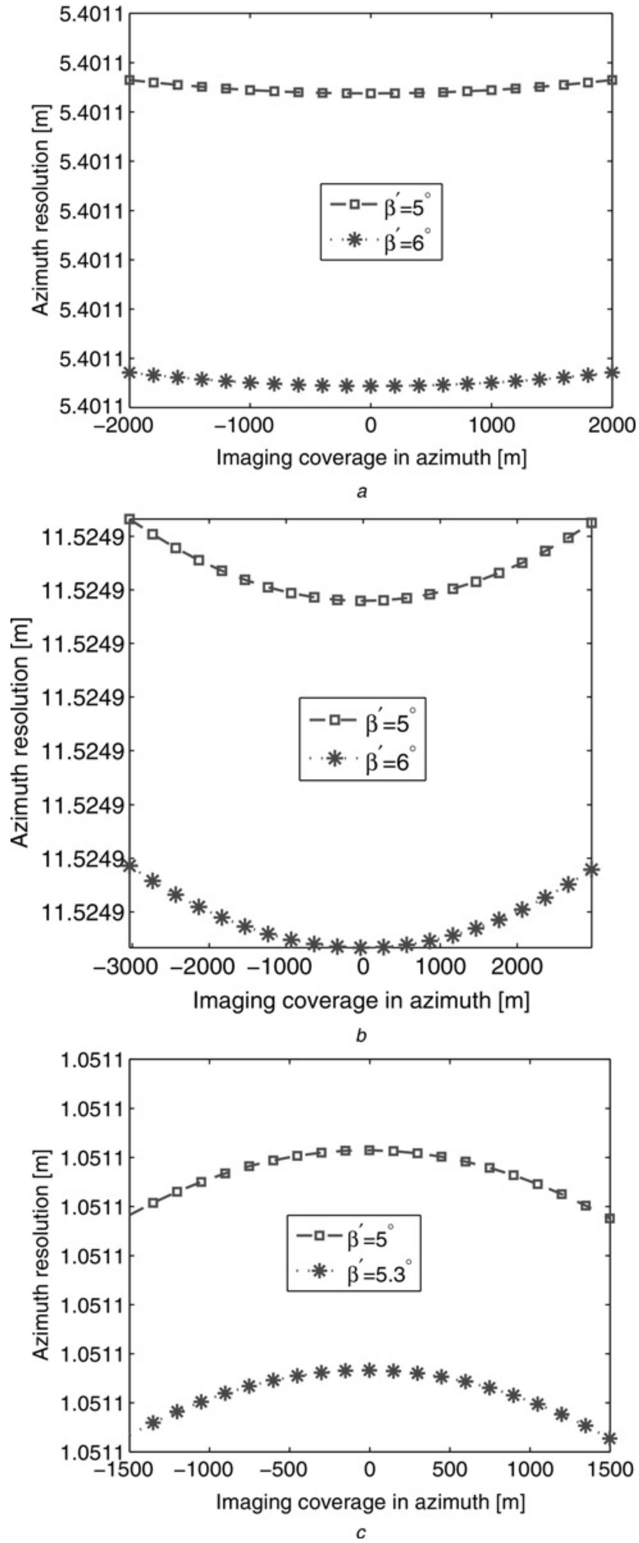

Fig. 8 *Azimuth resolution results of the example transmitter and receiver configurations*

a Case A: Tx-A and Rx-A
b Case B: Tx-B and Rx-B
c Case C: Tx-C and Rx-C

doi: 10.1049/iet-wss.2011.0178

Fig. 7 gives the range resolution results of the example radar sensor configurations. The range resolution has geometry-variant characteristics, which depends not only on slant range but also azimuth range. It degrades with the increase of azimuth range displaced from scene centre. To obtain a consistent range resolution, the imaged scene coverage should be limited or a long slant range should be employed. Fig. 8 gives the azimuth resolution results of the example radar sensor configurations. It can be noticed that the angle between the transmitter and the receiver velocity vectors has also an impact on the azimuth resolution. Additionally, we can notice that the azimuth resolution between scene centre and scene edge has a small performance difference. This phenomenon is caused by the change of azimuth time.

It is well known that the final imaging swath is inversely proportional to the height of the antenna aperture. To obtain a wider swath, the elevation dimension of the near-space vehicle-borne receive aperture should be in a small size. However, a smaller height of the transmit antenna implies a reduction on the radiometric resolution. Therefore, to further extend the imaging scene coverage, we present a multi-beamforming and scan-on-receive combined approach, as shown in Fig. 9. The receive antenna is formed by multiple channels or apertures in elevation and azimuth. The height of each receive subaperture should be small as soon as possible, each of them can cover a wide area illuminated by the spaceborne transmit aperture. The proper combination of the signals from the different channels is performed through a digital beamforming technique [37, 38], like the scan-on-receive discussed in [39]. The basic idea is to shape a time varying elevation beam in reception such that it follows the radar echoes on the ground.

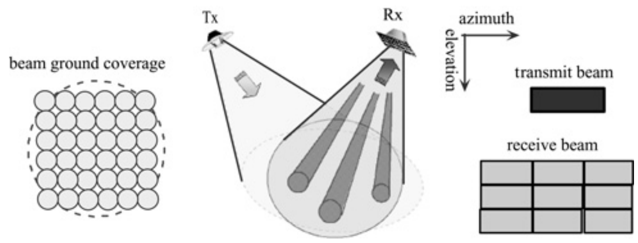

Fig. 9 *Extending imaged scene by using multi-beamforming and scan-on-receive combined approach*

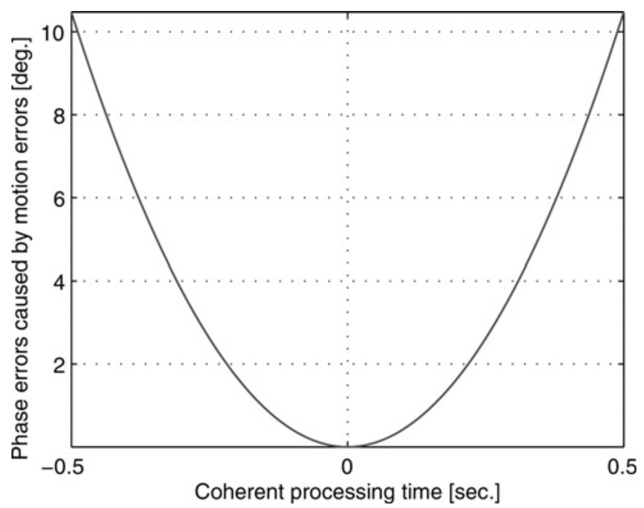

Fig. 10 *Assumed phase errors caused by the motion errors*

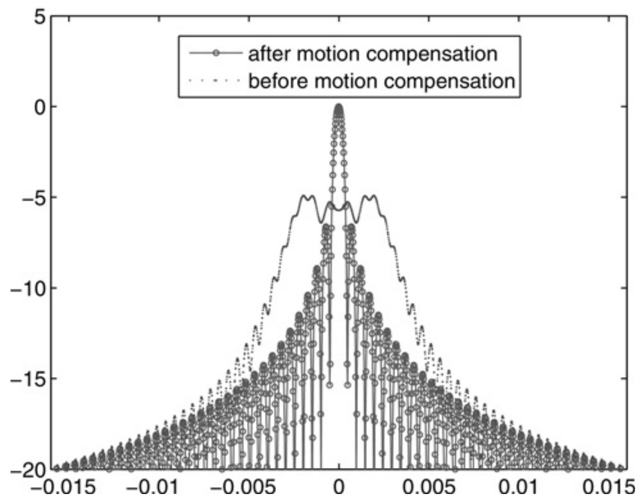

Fig. 11 *Comparative processing results between before and after applying the motion compensation algorithm*

To evaluate the performance of the overlapped subapertures-based motion compensation algorithm, we made a simulation using the following system parameters: radar carrier wavelength is $\lambda = 0.03$ m, a coherent processing interval is 1 s, the transmitter's speed is 7000 m/s, the distance from the transmitter to the target is 800 km, the ideal near-space vehicle-borne receiver's speed is 0 m/s and the distance from the receiver to the target is 30 km. We further assume there are phase errors caused by the motion errors as shown in Fig. 10. Fig. 11 shows the comparative processing results. It can be noticed that, after applying the motion compensation algorithm, significantly processing performance improvements are obtained.

5 Conclusion

This study proposes a distributed passive radar sensor network with near-space vehicle-borne receivers for regional remote sensing surveillance. We analysed the corresponding system performance such as imaging coverage and imaging resolution. Since there is a big-speed difference between the transmit and receive platforms, we proposed an approach to extend the imaging coverage through multi-beamforming and scan-on-receive. The numerical analysis results show that satisfactory imaging performance can be obtained by this approach. An overlapped subaperture-based motion compensation algorithm is also proposed for this passive radar sensor network, which is validated by the point target simulation results. Note that, in this study only one transmitter is employed. The radar sensor networks can employ multiple transmitters; however, in this case orthogonal waveforms may be required. Another remaining problem is synchronisation for distributed radar sensor networks. These problems will be further investigated in our subsequent work.

6 Acknowledgment

This work was supported in part by the National Natural Science Foundation of China under grant No. 41101317, the Fundamental Research Funds for the Central Universities under grant No. ZYGX2010J001, the First Grade of 49th Chinese Post-Doctor Research Funds under grant No. 20110490143 and the Open Funds of the State

Laboratory of Remote Sensing Science, Institute of Remote Sensing Applications, Chinese Academy of Sciences under grant No. OFSLRSS201011.

7 References

1 Arik, M., Akan, O.B.: 'Collaborative mobile target imaging in UWB wireless radar sensor networks', *IEEE J. Sel. Areas in Commun.*, 2010, **28**, (6), pp. 950–961
2 Liang, Q.L.: 'Radar sensor wireless channel modeling in Foliage environment: UWB versus narrowband', *IEEE Sensor J.*, 2011, **11**, (6), pp. 1448–1457
3 Schuerger, J., Garmatyuk, D.: 'Decteption jamming modeling in radar sensor networks'. Proc. IEEE Military Communications Conf., San Diego, CA, November 2008, pp. 1–7
4 Chiani, M., Giorgetti, A., Mazzotti, M., Minutolo, R., Paolini, E.: 'Target detection metrics and tracking for UWB radar sensor networks'. Proc. IEEE Int. Ultra-Wideband Conf., Vancouver, Canada, September 2009, pp. 469–474
5 Bartoletti, S., Conti, A., Giorgetti, A.: 'Analysis of UWB Radar Sensor Networks'. Proc. IEEE Int. Communication Conf., Cape Town, South Africa, May 2010, pp. 1–6
6 Bielefeld, D., Mathar, R., Hirsch, O., Thoma, R.S.: 'Power-aware distributed target detection in wireless sensor networks with UWB-radar nodes'. Proc. IEEE Radar Conf., Arlington, VA, May 2010, pp. 842–847
7 Xu, L., Liang, J.: 'Radar sensor network using a set of new ternary codes: theory and application', *IEEE Sensors J.*, 2011, **11**, (2), pp. 439–450
8 Jiang, D.D., Wang, L.: 'Communication networks mahalandobis distance-based traffic matrix estimation', *Eur. Trans. Telecommun.*, 2010, **21**, (3), pp. 195–201
9 Hume, A.L., Baker, C.J.: 'Netted radar sensing'. Proc. IEEE Radar Conf., Atlanta, GA, May 2001, pp. 23–26
10 Liang, Q.: 'Radar sensor networks for automatic target recognition with delay-Doppler uncertainty'. Proc. IEEE Military Commun. Conf., Washington, DC, June 2006, pp. 1–7
11 Liang, J., Liang, Q.: 'Design and analysis of distributed radar sensor networks', *IEEE Trans. Parallel Distrib. Syst.*, 2011, **22**, (11), pp. 1926–1933
12 Wang, W.Q.: 'Near-space vehicles: supply a gap between satellites and airplanes', *IEEE Aerosp. Electron. Syst. Mag.*, 2011, **25**, (4), pp. 4–9
13 Allen, E.H.: 'The case for near-space', *Aerosp. Am.*, 2006, **22**, (1), pp. 31–34
14 Tomme, E.B.: 'Balloons in today's military: an introduction to near-space concept', *Airspace J.*, 2005, **19**, (1), pp. 39–50
15 Wang, W.Q., Cai, J.Y., Peng, Q.C.: 'Near-space microwave radar remote sensing: potentials and challenge analysis', *Remote Sens.*, 2010, **2**, (3), pp. 717–739
16 Wang, W.Q., Cai, J.Y.: 'A technique for jamming bi- and multistatic SAR systems', *IEEE Geosci. Remote Sens. Lett.*, 2007, **4**, (1), pp. 80–82
17 Wang, W.Q.: 'Application of near-space passive radar for homeland security', *Sens. Imag.: An Int. J.*, 2007, **8**, (1), pp. 39–52
18 Wang, W.Q., Cai, J.Y., Peng, Q.C.: 'Near-space SAR: a revolutionizing remote sensing mission'. Proc. Asia-Pacific Synthetic Aperture Radar Conf., Huangshan, China, November 2007, pp. 127–131
19 Marcel, M.J., Baker, J.: 'Interdisciplinary design of a near-space vehicle'. Proc. IEEE Southeast Conf., Richmond, USA, March 2007, pp. 421–426
20 Guan, M.X., Guo, Q., Li, L.: 'A novel access protocol for communication system in near-space'. Proc. Wireless Communication Network Mobile Computation Conf., Shanghai, China, September 2007, pp. 1849–1852
21 Galletti, M., Krieger, G., Thomas, B., Marquart, M., Johannes, S.S.: 'Concept design of a near-space radar for tsunami detection'. Proc. IEEE Geosci. Remote Sens. Symp., Barcelona, June 2007, pp. 34–37
22 Rome, G., Frulla, G.: 'HELIPLAT: high altitude very-long endurance solar powered UAV for telecommunication and earth observation applications', *Aeronaut. J.*, 2004, **108**, (4), pp. 277–293
23 Wang, W.Q.: 'Near-space remote sensing: potential and challenges' (Springer, New York, 2011)
24 Krieger, G., Moreira, A.: 'Spaceborne bi- and multistatic SAR: potential and challenges', *IET Radar Sonar Navig.*, 2006, **153**, (3), pp. 184–198
25 Wang, W.Q.: 'GPS-based time & phase synchronization processing for distributed SAR', *IEEE Trans. Aerosp. Electron. Syst.*, 2009, **45**, (3), pp. 1040–1051
26 Lv, X., Xing, M., Wu, Y., Zhang, S.: 'Azimuth-invariant bistatic multichannel synthetic aperture radar for moving target detection and location', *IET Radar Sonar Navig.*, 2009, **3**, (5), pp. 461–473
27 Wang, W.Q., Ding, C.B., Liang, X.D.: 'Time and phase synchronization via direct-path signal for bistatic synthetic aperture radar systems', *IET Radar Sonar Navig.*, 2008, **2**, (1), pp. 1–11
28 Purdy, D.S.: 'Receiver antenna scan rate requirements needed to implement pulse chasing in a bistatic radar receiver', *IEEE Trans. Aerosp. Electron. Syst.*, 2001, **37**, (1), pp. 285–288
29 Gebhardt, U., Loffeld, O., Nies, H., Natroshvili, M., Knedlik, S.: 'Bistatic spaceborne/airborne experiment: geometrical modeling and simulation'. Proc. IEEE Int. Geosci. Remote Sens. Symp., Denver, July 2006, pp. 1832–1835
30 Willis, N.J.: 'Bistatic radar' (Artech House, 1991)
31 Walterscheid, I., Klare, J., Brenner, A.R., Ender, J.H.G., Loffeld, O.: 'Challenges of a bistatic spaceborne/airborne SAR experiment'. Proc. European Synthetic Aperture Radar Symp., Dresden, Germany, May 2006
32 Zhou, P., Pi, Y.M.: 'A technique for beam synchronization in non-cooperative hybrid bistatic SAR', *J. Electron. Inf. Tech.*, 2009, **31**, (5), pp. 1122–1126
33 Curlander, J.C., McDonough, R.N.: 'Synthetic aperture radar: systems and signal processing' (Wiley-Interscience, 1991)
34 Marcos, J.S., Dekker, P.L., Mallorqui, J.J., Aguasca, A., Prats, P.: 'SABRINA: a SAR bistatic receiver for interferometric applications', *IEEE Geosci. Remote Sens. Lett.*, 2007, **4**, (2), pp. 307–311
35 Lenz, R., Schuler, K., Younis, M., Wiesbeck, W.: 'TerraSAR-X active radar ground calibrator system', *IEEE Aerosp. Electron. Syst. Mag.*, 2006, **21**, (5), pp. 30–33
36 Liebe, J.R., van de Giesen, N., Andreini, M.S., Steenhuis, T.S., Walter, M.T.: 'Suitability and limitations of ENVISAT ASAR for monitoring small reservoirs in a semiarid area', *IEEE Trans. Geosci. Remote Sens.*, 2009, **47**, (5), pp. 1536–1547
37 Gebert, N., Krieger, G., Moreira, A.: 'Digital beamforming on receive: techniques and optimization strategies for high-resolution wide-swath SAR imaging', *IEEE Trans. Aerosp. Electron. Syst.*, 2009, **45**, (2), pp. 564–592
38 Younis, M., Fisher, C., Wiesbeck, W.: 'Digital beamforming in SAR systems', *IEEE Trans. Geosci. Remote Sens.*, 2003, **41**, (7), pp. 1735–1739
39 Suess, M., Grafmeller, R., Zahn, R.: 'A novel high resolution, wide swath SAR system'. Proc. IEEE Int. Geosci. Remote Sens. Symp., June 2001, pp. 1013–1015

doi: 10.1049/iet-wss.2011.0178